Proposal of 6th Radial Force Control Based on Flux Linkage
– Verification on Load Condition –

Masato Kanematsu, Takayuki Miyajima
Hiroshi Fujimoto, and Yoichi Hori
The University of Tokyo
5-1-5 Kashiwanoha,
Kashiwa, Chiba, 277-8561 Japan
kanematsu, miya@hflab.k.u-tokyo.ac.jp
fujimoto, hori@k.u-tokyo.ac.jp

Toshio Enomoto, Masahiko Kondou, Hiroshi Komiya
Kantaro Yoshimoto, and Takayuki Miyakawa
Nissan Motor Co., Ltd.
1-1, Morinosatoaoyama, Atsugi-shi
Kanagawa, 243-0123, Japan
enomoto, m-kondo, h-komiya@mail.nissan.co.jp
ka-yoshimoto, takayuki_miyakawa@mail.nissan.co.jp

***Abstract*— IPMSMs (Interior Permanent Magnet Synchronous Motors) are widely used for many industrial applications. However, IPMSMs cause large noise and vibration due to torque ripple and radial force. In this paper, 6th radial force modelling is constructed based on flux linkage and 6th radial force is controlled on the ground of this modelling. Firstly, we make some assumptions to lead 6th radial force modelling. Secondly, 6th radial force modelling is derived. Simulation results and Experimental results verify the validity of 6th radial force model. Finally, 6th radial force control is performed by injecting dq-axis harmonic current.**

I. INTRODUCTION

In many industrial applications, IPMSMs (Interior Permanent Magnet Synchronous Motors) are often selected as drive motors. In these applications, IPMSMs face strong demands about the reduction of noise and vibration. Specially the noise and vibration problems in the inside of cars remain to be one of the problems which should be solved. Furthermore lower acoustic noise and vibration is desirable to enhance the value of products[1].

The analysis technology on the vibration of electromagnetic force is investigated in [2][3][4] and [5]. The Reference [6] and [7] propose the designing method to reduce radial force vibration. It is natural to apply skew method for reducing the vibration of radial force [8][9][10]. However, the methods with structual designing usually increase the cost of the products. We therefore focus on the method to reduce radial force with current control. The Reference [11] proposes the control method to suppress harmonic radial force with harmonic current. However, this method needs iterative calculations of electromagnetic field analysis in each drive condition and how to lead optimal reference to suppress radial force is unclear.

It is known that in IPMSMs electrical 2nd and 6th radial forces usually cause serious noise and vibration. It is known that there exist phase differences between the 2nd radial force on U, V and W-phase tooth as:

$$F_{rU}(\theta) = F_{r2}\cos 2\theta \quad (1)$$

$$F_{rV}(\theta) = F_{r2}\cos 2\left(\theta - \frac{2}{3}\pi\right) \quad (2)$$

$$F_{rW}(\theta) = F_{r2}\cos 2\left(\theta - \frac{4}{3}\pi\right) \quad (3)$$

where F_{r2} is the amplitude of 2nd radial force. This causes Pth order annular elastic deformation, where P denotes pole pairs. 2nd radial froce modelling and control method have been proposed in [15]. On the other hand, 6th radial forces on U, V and W-phase tooth are in phase as:

$$F_{rU}(\theta) = F_{r6}\cos 6\theta \quad (4)$$

$$F_{rV}(\theta) = F_{r6}\cos 6\left(\theta - \frac{2}{3}\pi\right) \quad (5)$$

$$F_{rW}(\theta) = F_{r6}\cos 6\left(\theta - \frac{4}{3}\pi\right) \quad (6)$$

Therefore the transfer characteristics from radial force to acceleration has very high amplitude because 6th radial force excites spatially 0th annular mode. Fig. 1 shows the concept of 2nd and 6th radial force and typical natural frequency mode of the stator.

In this paper, 6th component of the radial force on a tooth is expressed mathematically based on flux linkage. This expression clarifies the relationship between dq-axis harmonic current and 6th radial force and enables us to control 6th radial force. The simulation and experiment are performed to validate the utility of the modelling and suppression control method.

II. ASSUMPTION OF APPROXIMATION

In this chapter, assumption of approximation are shown. Based on these assumptions, approximation model of 6th radial force is derived. JMAG (electromagnetic field analysis software) produced by JSOL Corporation is utilized for this analysis.

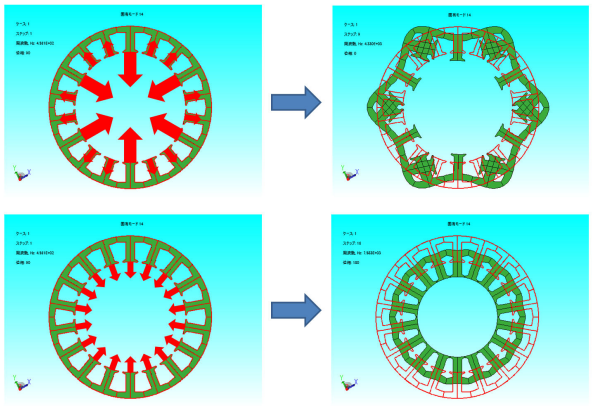

Fig. 1. Typical natural frequency mode of stator(12P18S)

A. The relationship between current, flux linkage and radial force

Flux linkage through a U-phase tooth $\phi_u(t)$ is expressed as

$$\phi_u(t) = \frac{\psi_u(t)}{N} \tag{7}$$

where, N is turn number per a phase and ψ_u is flux linkage on U-phase tooth.

We assume the tangential flux distribution $B_\theta(t)$ is small, and all flux linkage is generated by the radial flux distribution $B_r(t)$.

$$\phi_u(t) = \int B_r(t) dS \tag{8}$$

Radial force on a U-phase tooth $f_u(t)$ is calculated based on Maxwell stress.

$$f_u(t) = \int \frac{B_r(t)^2}{2\mu_0} dS \tag{9}$$

where S is a tooth area facing air region. This paper has the assumption that flux is distributed equally over the tooth area S. With this assumption, (8) and (9) are rewritten as (10) and (11).

$$\phi_u(t) = B_r(t) S \tag{10}$$

$$f_u(t) = \frac{B_r^2(t)}{2\mu_0} S \tag{11}$$

In this paper, we consider constant speed condition and radial force is regarded as a function for electrical angle θ. Substituting (7) and (10) into (11), equation (12) is obtained.

$$f_u(\theta) = \frac{\psi_u^2(\theta)}{2\mu_0 S N^2} = A\psi_u^2(\theta) \tag{12}$$

$$A := \frac{1}{2\mu_0 S N^2} \tag{13}$$

(12) is called the approximation of radial force in this paper.

B. Assumption on flux linkage

It is also assumed that flux linkage caused by permanent magnet $\psi_{um}(\theta)$ and flux linkage caused by current $\psi_{ui}(\theta)$ satisfy linear independency.

$$\psi_u(\theta) = \psi_{um}(\theta) + \psi_{ui}(\theta) \tag{14}$$

This paper considers 12 poles 18 slots IPMSM. The winding pattern is concentrated winding. To consider 6th radial force, $\psi_{um}(\theta)$ is defined as:

$$\psi_{um}(\theta) = \psi_{1m}\cos\theta + \psi_{5m}\cos 5\theta + \psi_{7m}\cos 7\theta \tag{15}$$

5th and 7th flux linkage ψ_{5m} and ψ_{7m} have negative value when they have opposite phase against fundamental flux linkage. On ground of the symmetry, flux linkage on U-phase tooth is considered. The parameter of IPMSM is shown in Table I. dq-axis current reference i_d, i_q is defined as :

$$i_d := I_{d0} + i_{d6} \tag{16}$$

$$i_{d6} := I_{d6}\cos(6\theta - \theta_{d6}) \tag{17}$$

$$i_q := I_{q0} + i_{q6} \tag{18}$$

$$i_{q6} := I_{q6}\cos(6\theta - \theta_{q6}) \tag{19}$$

TABLE I
PARAMETERS OF IPMSM

turn number N	120
a pair of poles P	6
teeth area S [m^2]	4.13×10^{-4}
ψ_{m1}[mWb]	36.2
ψ_{m5}[mWb]	0.811
ψ_{m7}[mWb]	-0.114
L_d[mH]	0.866
L_q[mH]	1.31

III. THE INFLUENCE OF d-AXIS HARMONIC CURRENT

Flux linkage on U-phase caused by d-axis harmonic current ψ_{uih} is shown as:

$$\begin{bmatrix}\psi_{uih}\\ \psi_{vih}\\ \psi_{wih}\end{bmatrix} = \boldsymbol{C}_{dq}^{uvw}\begin{bmatrix}L_d I_{d6}\cos(6\theta - \theta_{d6})\\ 0\end{bmatrix}$$

$$= \sqrt{\frac{1}{6}} L_d I_{d6}\begin{bmatrix}\cos(5\theta - \theta_{d6}) + \cos(7\theta - \theta_{d6})\\ \cos(5\theta - \theta_{d6} + \frac{2}{3}\pi) + \cos(7\theta - \theta_{d6} - \frac{2}{3}\pi)\\ \cos(5\theta - \theta_{d6} + \frac{4}{3}\pi) + \cos(7\theta - \theta_{d6} - \frac{4}{3}\pi)\end{bmatrix} \tag{20}$$

Adding harmonic flux linkage ψ_{uih}, all flux linkage on U-phase is written by :

$$\begin{aligned}\psi_u(\theta) =& \sqrt{\frac{2}{3}}(\Psi_{1m} + L_d I_{d0})\cos\theta - \sqrt{\frac{2}{3}} L_q I_{q0}\sin\theta\\ &+ \psi_{5m}\cos 5\theta + \sqrt{\frac{1}{6}} L_d I_{d6}\cos(5\theta - \theta_{d6})\\ &+ \psi_{7m}\cos 7\theta + \sqrt{\frac{1}{6}} L_d I_{d6}\cos(7\theta - \theta_{d6})\end{aligned} \tag{21}$$

where, $\Psi_{1m} := \sqrt{\frac{3}{2}}\psi_{1m}$. In this paper, 2-phase/3-phase transform is absolute transformation. Substituting (21) into (12), the 6th order component generated by d-axis harmonic

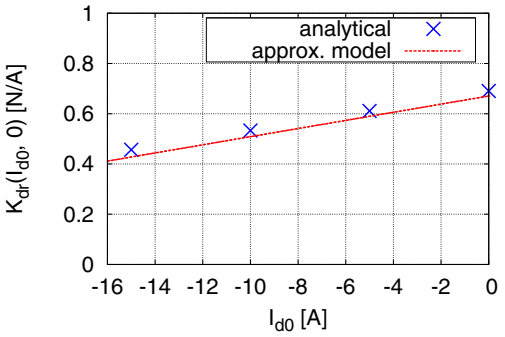

(a) $K_{dr}(I_{d0}, 0)$ when I_{d0} varies

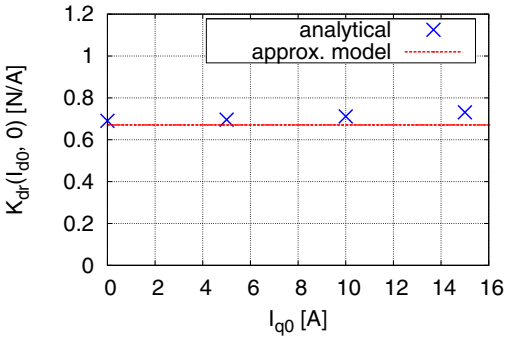

(b) $K_{dr}(0, I_{q0})$ when I_{q0} varies

Fig. 2. The comparison between $K_{dr}(I_{d0}, I_{q0})$ and FEA results

current is extracted as :

$$f_{i_{d6}}(I_{d0}, I_{q0}, I_{d6}, \theta_{d6}) = \frac{A}{3}(\Psi_{1m} + L_d I_{d0}) L_d I_{d6} \cos(6\theta - \theta_{d6}) \quad (22)$$
$$= K_{dr}(I_{d0}, I_{q0}) i_{d6}$$

$$K_{dr}(I_{d0}, I_{q0}) := \frac{A}{3}(\Psi_{1m} + L_d I_{d0}) L_d \quad (23)$$

where $f_{i_{d6}}(I_{d0}, I_{q0}, I_{d6}, \theta_{d6})$ is 6th radial force caused by i_{d6}. To verify the accuracy of (22), FEA is performed on the condition that $I_{d6} = 1$A and $\theta_{d6} = 0$deg. The FEA result is shown in Fig.2. Although a lot of assumptions have been made to lead (22), we can see that 6th radial force model (22) differs very little from FEA result.

IV. The Influence of q-axis Harmonic Current

In the same way, flux linkage generated by q-axis harmonic current $\psi_{uih}(\theta)$ is calculated as:

$$\begin{bmatrix} \psi_{uih}(\theta) \\ \psi_{vih}(\theta) \\ \psi_{wih}(\theta) \end{bmatrix} = \boldsymbol{C}_{dq}^{uvw} \begin{bmatrix} 0 \\ L_q I_{q6} \cos(6\theta - \theta_{q6}) \end{bmatrix}$$
$$= \sqrt{\frac{1}{6}} L_q I_{q6} \begin{bmatrix} \sin(5\theta - \theta_{q6}) - \sin(7\theta - \theta_{q6}) \\ \sin(5\theta - \theta_{q6} + \frac{2}{3}\pi) - \sin(7\theta - \theta_{q6} - \frac{2}{3}\pi) \\ \sin(5\theta - \theta_{q6} + \frac{4}{3}\pi) - \sin(7\theta - \theta_{q6} - \frac{4}{3}\pi) \end{bmatrix} \quad (24)$$

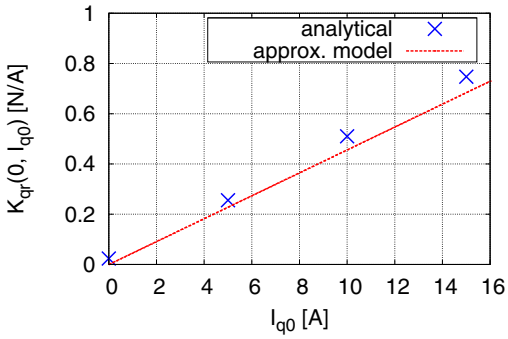

Fig. 3. $F_{i_{q6}}(0, I_{q0})$ when I_{q0} varies

Substituting (24) into (12), the 6th order component generated by q-axis harmonic current is extracted as:

$$f_{i_{q6}}(I_{d0}, I_{q0}) = \frac{A}{3} L_q I_{q0} L_q I_{q6} \cos(6\theta - \theta_{q6}) \quad (25)$$
$$= K_{qr}(I_{d0}, I_{q0}) i_{q6} \quad (26)$$

$$K_{qr}(I_{d0}, I_{q0}) := \frac{A}{3} L_q^2 I_{q0} \quad (27)$$

Fig.3 shows the FEA results which are performed on the condition that $I_{q6} = 1$A, $\theta_{q6} = 0$A, and $I_{d0} = 0$A. Fig.3 shows that Eq. (27) can predict 6th radial force caused by q-axis harmonic current well.

A. 6th radial force control

The transfer characteristics between 6th harmonic current and 6th radial force have been obtained. All 6th radial force is expressed as

$$f_{r6}(i_d, i_q) = f_{\text{base}}(I_{d0}, I_{q0}) + K_{dr}(I_{d0}, I_{q0}) i_{d6} + K_{qr}(I_{d0}, I_{q0}) i_{q6} \quad (28)$$

$$f_{\text{base}}(I_{d0}, I_{q0}) := F_{\text{base}} \cos(6\theta - \theta_{\text{base}}) \quad (29)$$

where $f_{\text{base}}(I_{d0}, I_{q0})$ is 6th radial force caused by harmonic inductance and harmonic magnetic flux. $f_{\text{base}}(I_{d0}, I_{q0})$ varies according to I_{d0} and I_{q0}. $f_{\text{base}}(I_{d0}, I_{q0})$ can be obtained by calculating 6th radial force without harmonic current in FEA. With $F_{\text{base}}(I_{d0}, I_{q0})$ and $\theta_{\text{base}}(I_{d0}, I_{q0})$, 6th harmonic current reference is obtained as

$$i_{d6:\text{opt}} = -\frac{F_{\text{base}}(I_{d0}, I_{q0})}{K_{dr}(I_{d0}, I_{q0})} \cos(6\theta - \theta_{\text{base}}(I_{d0}, I_{q0})) \quad (30)$$

$$i_{q6:\text{opt}} = -\frac{F_{\text{base}}(I_{d0}, I_{q0})}{K_{qr}(I_{d0}, I_{q0})} \cos(6\theta - \theta_{\text{base}}(I_{d0}, I_{q0})) \quad (31)$$

Fig. 4 shows simulation result of 6th radial force control by d-axis harmonic current. 4th and 8th radial forces are affected by 6th d-axis current because 5th and 7th harmonic fluxes generated by 5th and 7th harmonic current produce 4th and 8th radial forces. However, considering transfer characteristics of 4th and 8th radial forces, which has Pth annular mode, it is said that 4th and 8th radial forces cause little noise and

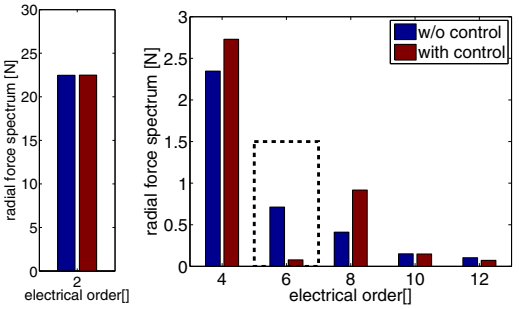

(a) 2nd (b) 4-12th order

Fig. 4. 6th radial force control by d-axis harmonic current(simulation result)

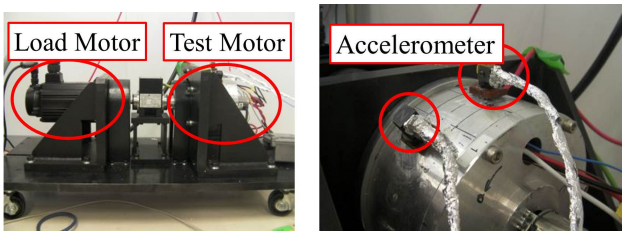

(a) Test motor and load motor (b) Accelerometer

Fig. 5. Experimental environment

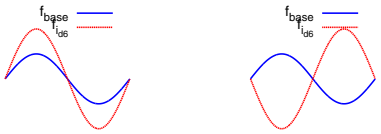

(a) θ_{d6} = 30 deg(Fig. 6(a)) (b) θ_{d6} = 210 deg(Fig. 6(a))

Fig. 7. The phase relationship between $f_{\rm base}$ and $f_{i_{d6}}$ in Fig. 6(a)

vibration.

V. Experimental Results

In experiment, radial acceleration on the surface of test motor is evaluated intead of radial force. The speed of the test motor is controlled as 800rpm by load motor. Fig. 5 shows test motor, load motor and accelerometer. The current controller is designed as Perfect Tracking Control and Pole zero cancellation PI Control[16]. 6th radial acceleration $a_{r6}(\omega)$ is expressed theoretically as

$$a_{r6}(\omega) = H(\omega) f_{r6}(i_d, i_q). \tag{32}$$

where $H(\omega)$ is transfer characteristics between radial force and vibratoin at the speed of ω.

A. The validation of approximation model

To validate the approximation model (22) and (26), some expreriments are performed. At first, 6th radial acceleration is shown in 6(a) under the condition that I_{d6} = 2.5A, I_{q6} = 0A, I_{d0} = 0A and I_{q0}, $\theta_{i_{d6}}$ vary. It can be seen in Fig. 6(a) that the phase of 6th radial force is varied by shifting the phase of d-axis harmonic current. In the result, when $f_{\rm base}$ is opposite to $\theta_{i_{d6}}$ 6th radial acceleration decreases and when $f_{\rm base}$ corresponds to $\theta_{i_{d6}}$ 6th radial acceleration increases in Fig. 6(a). Fig. 7 shows the situation when I_{q0} is 5A and θ_{d6} is 30 and 210deg in Fig. 6(a). $\theta_{\rm base}$ is identified as 30deg from Fig. 6(a) in this drive condition. In Fig. 6(b), the result of d-axis 6th harmonic current effect to acceleration is shown. The fact that 6th radial acceleration caused by d-axis harmonic current $a_{i_{d6}}$ is independent of θ_{d6} and I_{q0} validates the approximation model (22).

The transfer characteristics of radial acceleration from d-axis 6th harmonic current $H(\omega_0)K_{dr}(I_{d0}, I_{q0})$ is identified as

$$(H(\omega_0)K_{dr}(0,5))' = 1.35 \times 10^{-2}[\mathrm{m/s^2}/A] \tag{33}$$

because in Fig. 6(b) the average acceleration of $a_{i_{d6}}$ is $3.37 \times 10^{-2} m/s^2$, which is generated by I_{d6} of 2.5A. In Eq. (33), the symbol of $()'$ denotes the parameter indentified by the experiment.

In the same way, Fig. 6(c) shows the experimental results when I_{d6} = 0A, I_{q6} = 2.5A, I_{d0} = 0A and I_{q0}, $\theta_{i_{q6}}$ vary. In Fig. 6(d), the result of q-axis 6th harmonic current effect to acceleration is shown. Eq. (26) indicates that the average acceleration at I_{q0} = 10A is twice as large as the average acceleration at I_{q0} = 5A. In Fig. 6(d) the average acceleration at I_{q0} = 10A is one point three larger than that at I_{q0} = 5A.

The transfer characteristics of radial acceleration is obtained as

$$(H(\omega_0)K_{qr}(0,5))' = 2.26 \times 10^{-2}[\mathrm{m/s^2}/A]. \tag{34}$$

B. The result of 6th radial force control

In this chapter, 6th radial force control is realized under the condition that the rotation speed is 800rpm, I_{d0} is 0A, and I_{q0} is 5A. In this section, to maximize the effect of 6th radial force control, the current references of 6th radial force control are identified by experiment.

At first, 6th radial acceleration $a_{r6}(I_{d0}, I_{q0})$ is measured with keeping harmonic current zero.

$$(H(\omega_0)F_{\rm base}(I_{d0}, I_{q0}))' = a_{r6}(I_{d0}, I_{q0}) \tag{35}$$

Experimental results is shown in Fig. 8(a) 8(d) 8(g) 8(j) 8(m), where to make discussions the output of torque meter and theta acceleration are shown. $(H(\omega_0)F_{\rm base}(0,5))'$ is identified by 6th radial acceleration in Fig. 8(a) as:

$$(H(\omega_0)F_{\rm base}(0,5))' = 2.97 \times 10^{-2}[\mathrm{m/s^2}] \tag{36}$$

With Eq. (33) and (34), dq-axis harmonic current references are calculated as:

$$i_{d6:\rm opt} = -\frac{(H(\omega_0)F_{\rm base}(0,5))'}{(H(\omega_0)K_{dr}(0,5))'}\cos(6\theta - \theta_{\rm base}) \tag{37}$$

$$i_{q6:\rm opt} = -\frac{(H(\omega_0)F_{\rm base}(0,5))'}{(H(\omega_0)K_{qr}(0,5))'}\cos(6\theta - \theta_{\rm base}) \tag{38}$$

$$i_{d6:\rm opt} = -2.20\cos\left(6\theta - \frac{1}{6}\pi\right) \tag{39}$$

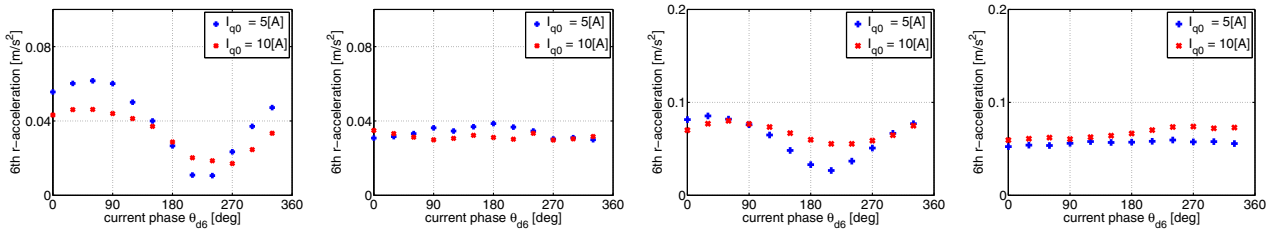

(a) a_{r6} with injecting i_{d6} (b) $a_{i_{d6}}$ (c) a_{r6} with injecting i_{q6} (d) $a_{i_{q6}}$

Fig. 6. The validation of approximation model(Experimental result)

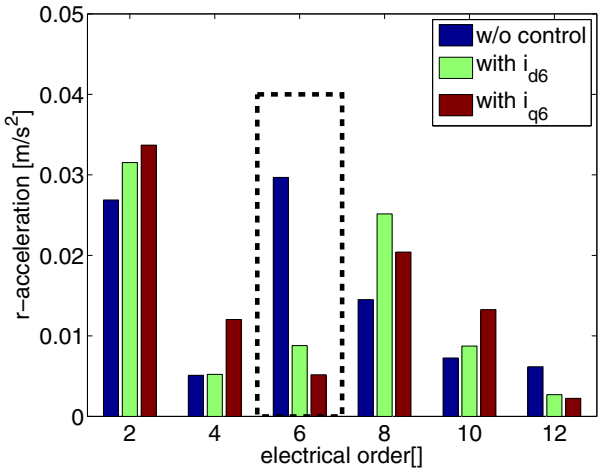

Fig. 9. The comarison of 6th radial force controls(Experimental Result)

$$i_{q6:\mathrm{opt}} = -1.31\cos\left(6\theta - \frac{1}{6}\pi\right) \tag{40}$$

Fig. 8 shows the result of 6th radial force control by $i_{d:\mathrm{opt}}$ and $i_{q:\mathrm{opt}}$.

6th radial accelerations caused by 6th radial force are largely suppressed in Fig. 8(b) and 8(c). when $i_{q6:\mathrm{opt}}$ are selected to suppress radial force, 6th circumferential acceleration caused by torque ripple increases in Fig. 8(f). On the other hand, there are little deterioration of 6th circumferential acceleration with $i_{d6:\mathrm{opt}}$ in Fig. 8(e). Fig. 9 shows the comparison of radial acceleration with 6th radial force control. It is notable that the decrease of 6th radial acceleration is larger than the increase of 4th and 8th radial accelerations.

VI. CONCLUSION

In this paper, we proposed the modelling of 6th radial force caused by dq-axis harmonic current based on flux linkage. This model enables us to evaluate the harmonic radial force generated by dq-axis harmonic current. The validity of the proposed model were verified by FEA and experiment. Based on this modelling, 6th radial force was suppressed. In our future works, 6th radial force control combined with dq-axis harmonic current will be proposed to suppress both circumferential and radial acceleration.

REFERENCES

[1] Kondo Keiichiro,Kubota Hisao: "Innovative Application Technologies of AC Motor Drive Systems" IEEJ Trans. Industry Applications, Vol.1, No.3 pp.132-140(2012)

[2] M.Islam, R.Islam, T.Sebastian : "Noise and vibration characteristics of permanent magnet synchronous motors using electromagnetic and structural analyses", IEEE International Conference on Energy Conversion Congress and Exposition (ECCE), Vol.17, No.22, pp.3399-3405,2011

[3] H.Y.Issac Du, Lei Hao, and Hejie Lin: "Modeling and analysis of electromagnetic vibrations in fractional slot PM machines for electric propulsion," Energy Conversion Congress and Exposition (ECCE), pp.5077-5084(2013)

[4] J.F. Gieras, Chong Wang, Joseph. C.S.Lai, Nesimi Ertugrul: "Analytical Prediction of Noise of Magnetic Origin Produced by Permanent Magnet Brushless Motors," IEEE International Conference on Electric Machines Drives Conference(IEMDC), Vol.1, No.5, pp.148-152(2007)

[5] M. Boesing, R.W. De Doncker: "Exploring a Vibration Synthesis Process for the Acoustic Characterization of Electric Drives" IEEE Trans. Ind. Appl., vol.48, no.1, pp.70-78(2012)

[6] T.Kobayashi, Y.Takeda, M.Sanada, and S.Morimoto: "Vibration Reduction of IPMSM with Concentrated Winding by Making Holes", IEEJapan Trans. D, Vol. 124-D, No.2, pp. 202-207, 2004(in Japanese).

[7] Sang-Ho Lee, Jung-Pyo Hong, Sang-Moon Hwang, Woo-Taik Lee, Ji-Young Lee, Young-Kyoun Kim: "Optimal Design for Noise Reduction in Interior Permanent-Magnet Motor", IEEE Trans. Ind. Appl., vol.45, no.6, pp.1954-1960, Nov.-dec. 2009

[8] D. C. Hanselman: "Effect of skew, pole count and slot count on brushless motor radial force, cogging torque and back EMF", Inst. Elect. Eng. Proc. mdash,Elect. Power Appl., Vol.144, No.5, pp.325-330, 1997

[9] Jae-Woo Jung; Do-Jin Kim; Jung-Pyo Hong; Geun-Ho Lee; Seong-Min Jeon: "Experimental Verification and Effects of Step Skewed Rotor Type IPMSM on Vibration and Noise", IEEE Trans. Magn., vol.47, no.10, pp.3661-3664, 2011

[10] A. Cassat, C. Espanet, R. Coleman, L. Burdet, E. Leleu,D. Torregrossa, J. M' Boua, A. Miraoui: "A Practical Solution to Mitigate Vibrations in Industrial PM Motors Having Concentric Windings", IEEE Trans. Ind. Appl., vol.48, no.5, pp.1526-1538, 2012

[11] W. Zhu, B. Fahimi, and S. Pekarek, gA field reconstruction method for optimal excitation of surface mounted permanent magnet synchronous machines,h IEEE Trans. Energy Convers., vol. 21, no. 2, pp. 303-313, Jun. 2006.

[12] Jae-Woo Jung, Do-Jin Kim, Jung-Pyo Hong, Geun-Ho Lee, Seong-Min Jeon: "Experimental Verification and Effects of Step Skewed Rotor Type IPMSM on Vibration and Noise," IEEE Trans. Magnetics, Vol.47, No.10, pp.3661-3664(2011)

[13] Tao Sun, Ji-Min Kim, Geun-Ho Lee, Jung-Pyo Hong, Myung-Ryul Choi: "Effect of Pole and Slot Combination on Noise and Vibration in Permanent Magnet Synchronous Motor", IEEE Trans. Magnetics, Vol.47, No.5, pp.1038-1041(2011)

[14] Jiao Guandong, C.D.Rahn : "Field weakening for radial force reduction in brushless permanent-magnet DC motors" IEEE Trans. Magnetics, Vol.40, No.5, pp. 3286- 3292(2004)

[15] M.Kanematsu, T.Miyajima, H.Fujimoto, Y.Hori, T.Enomoto, M.Kondou, H.Komiya, K.Yoshimoto, T.Miyakawa: "Suppression Control of Radial Force Vibration due to Fundamental Permanent-Magnet Flux in IPMSM", IEEE Energy Conversion Congress and Exposition(ECCE), pp.2812-2816 (2013)

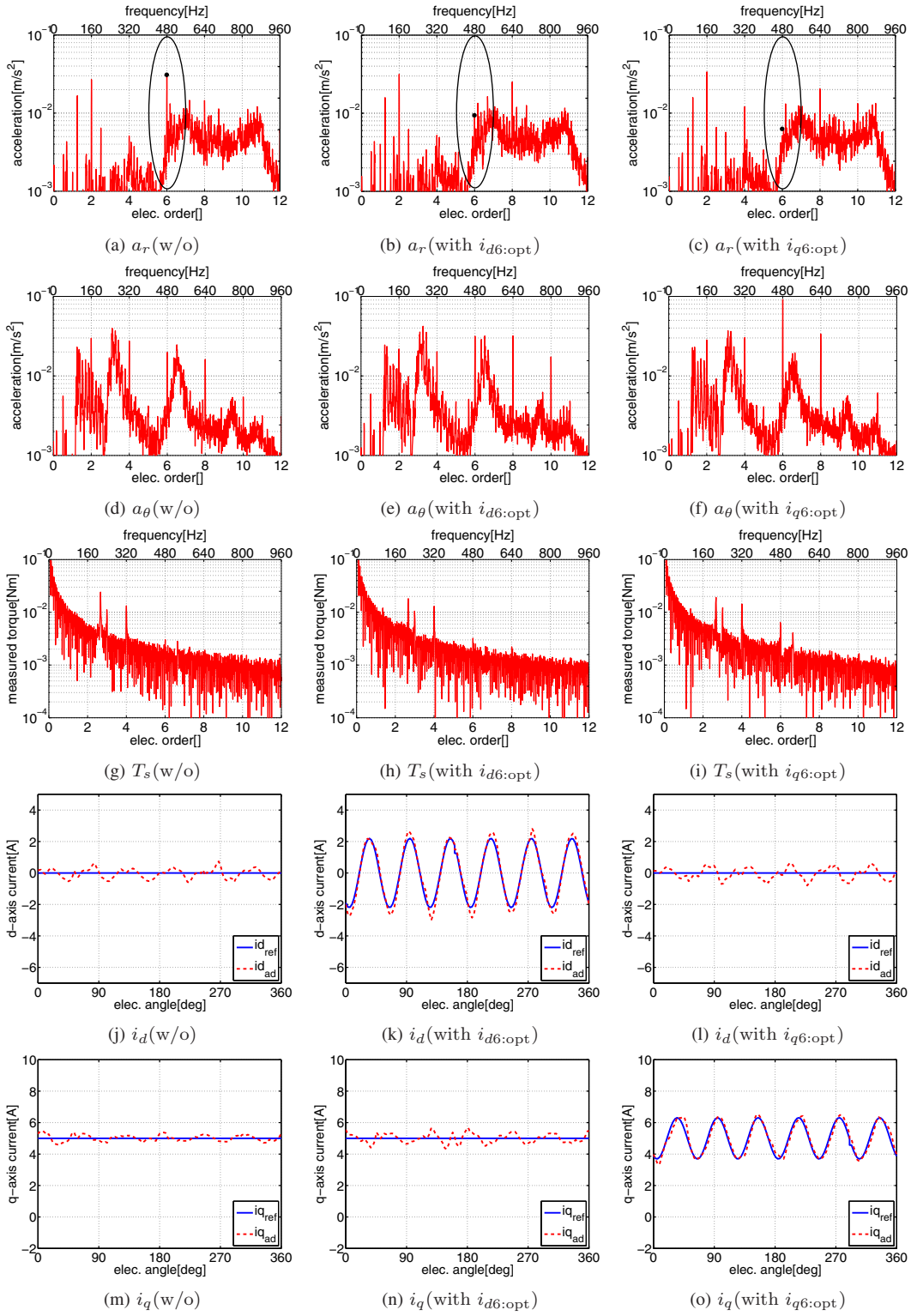

(a) a_r(w/o) (b) a_r(with $i_{d6:\mathrm{opt}}$) (c) a_r(with $i_{q6:\mathrm{opt}}$)

(d) a_θ(w/o) (e) a_θ(with $i_{d6:\mathrm{opt}}$) (f) a_θ(with $i_{q6:\mathrm{opt}}$)

(g) T_s(w/o) (h) T_s(with $i_{d6:\mathrm{opt}}$) (i) T_s(with $i_{q6:\mathrm{opt}}$)

(j) i_d(w/o) (k) i_d(with $i_{d6:\mathrm{opt}}$) (l) i_d(with $i_{q6:\mathrm{opt}}$)

(m) i_q(w/o) (n) i_q(with $i_{d6:\mathrm{opt}}$) (o) i_q(with $i_{q6:\mathrm{opt}}$)

Fig. 8. 6th radial force controliExperimental Resultj

[16] K.Nakamura, H.Fujimoto, M.Fujitsuna: ”Torque ripple suppression control for PM motor with current control based on PTC”, Power Electronics Conference (IPEC), 2010 International , pp.1077-1082, June 2010